Time-resolved contrast function and optical characterization of spatially varying absorptive inclusions at different depths in diffusing media

S. De Nicola
Istituto di Cibernetica del CNR "E. Caianiello," compr. A. Olivetti, Via Campi Flegrei 34, 80078 Pozzuoli, Italy

R. Esposito*
Dipartimento Scienze Fisiche, Università "Federico II," Napoli, Italy
and Istituto Nazionale di Fisica della Materia, Unità di Napoli, Napoli, Italy

M. Lepore
Dipartimento di Medicina Sperimentale, Seconda Università di Napoli, Napoli, Italy

P. L. Indovina
Dipartimento Scienze Fisiche, Università "Federico II," Napoli, Italy
and Istituto Nazionale di Fisica della Materia, Unità di Napoli, Napoli, Italy
(Received 1 August 2003; published 4 March 2004)

The role of a spatially varying absorptive inhomogeneity located at different depths within a turbid material has been investigated. This inhomogeneity has been characterized by a spatially dependent Gaussian distribution of its absorption coefficient. The present study has been performed calculating the time-resolved contrast function in the framework of the first-order perturbative approach to the diffusion equation for a slab geometry and a coaxial measurement scheme. The model has allowed us to take into account different locations of the inclusion along the source-detector axis. The accuracy of time-resolved contrast predictions has been analyzed through comparisons with results of the finite element method that has been used to numerically solve the diffusion equation. Recovery of the absorption perturbation parameter of the inhomogeneity for different axial positions has also been investigated.

DOI: 10.1103/PhysRevE.69.031901 PACS number(s): 87.10.+e, 42.25.Dd, 42.62.Be

I. INTRODUCTION

Optical imaging of objects hidden inside highly scattering media is a growing research activity in the biomedical applications area. Safe and noninvasive imaging modalities with diagnostic ability can be developed using near infrared light in the framework of diffusion approximation [1]. The functional imaging of the brain and the detection of breast tumors are the current aims of optical imaging [2,3]. Such applications are intensely pursued using time-domain, frequency-domain, and continuous wave methods to measure the transmission light between points on the sample surface [4–6]. So far, two general approaches have been considered for imaging: optical tomography and two-dimensional image projection. Optical tomography-based techniques aim at generating a three-dimensional (3D) map of the absorption and scattering coefficients within the turbid medium under investigation by using more or less complex source-detector measurement schemes and 3D inversion algorithms [3,7,8]. Generally, these inversion procedures are computationally expensive to handle a large amount of data, and novel linear perturbation approaches have been recently proposed to greatly reduce the computation time [9–11]. On the other hand, projection techniques provide two-dimensional images by a coaxial scanning of the sample slightly compressed between parallel planes with a source-detector pair in a tandem geometry [12–15]. This approach is currently employed in clinical applications for breast tumor detection and it relies on the basis of recovering the different optical properties of normal and pathological tissues from analytical expressions that fit transmittance measurements.

Analytical expressions for the time-resolved transmittance and reflectance have been obtained [16–18] for simple geometries such as an infinitely extended homogeneous scattering slab of a given thickness. Since the slab can be considered a good model for biomedical applications such as a compressed breast, solutions of the time-dependent diffusion equation for this simple geometry are of valuable practical interest [19,20], inasmuch as the diffusion equation-based model is adequate for describing photon migration in optically thick tissues. However, analytical solutions that account for the effect of an inclusion on the light propagation in an otherwise homogeneous turbid medium cannot be obtained in general. Consequently, perturbation-based schemes that give results as accurate as possible are adopted. In this regard, first-order perturbation expressions for the diffuse reflectance and transmittance have been obtained in the case of a small inclusion with spatially uniform optical properties that slightly differ from those of the host medium [15,21–24]. Small inclusion means neglecting the change of fluence rate in the region of the inhomogeneity at first-order approximation. Models have been tested on tissue phantoms recovering absolute optical properties of the inclusions. Obviously, the reconstructed values are more accurate when the perturbation is small, which is not always the case in real life

*Electronic address: rosesp@na.infn.it

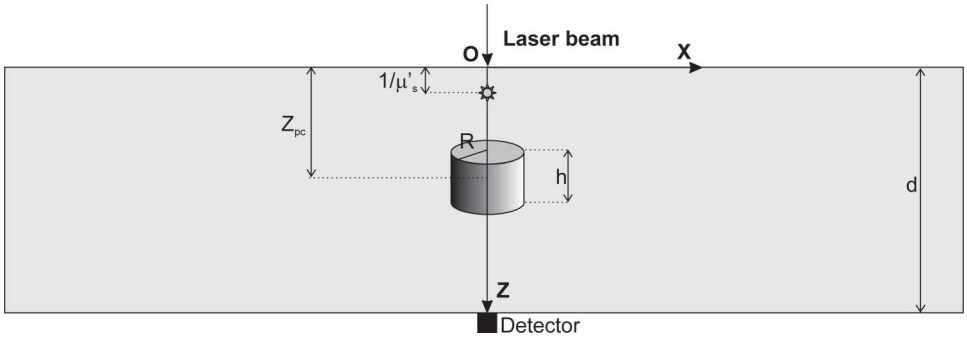

FIG. 1. Geometric scheme assumed for the perturbation model. A Gaussian absorptive inclusion of cylindrical shape geometry with radius R and height h is centered at $z=z_{pc}$ inside a turbid slab of thickness d. A pulsed light beam illuminates the front surface of the scattering slab at plane $z=0$. The photons are assumed to be initially isotropically scattered at a depth $z_s=1/\mu_s'$ below the front surface. The time-resolved transmittance is measured by a detector at plane $z=d$ coaxial with the source and with the inclusion.

applications. In order to extend the range of validity to larger volumes an empirical correction to the diffusion perturbation models has been proposed in Ref. [25].

Recently, we have developed [26] a perturbation model that accounts for the effect of spatially varying optical parameters of an inclusion on the time-resolved transmittance. We have analyzed the case of a Gaussian absorptive inclusion located at the central plane of a scattering slab in coaxial detection. The time-resolved contrast function computed by the perturbation model has been compared with one of the finite element method (FEM) simulations that have been used to numerically solve the diffusion equation in the presence of the spatially varying Gaussian absorptive inclusion. The analysis has showed that the change in transillumination signals resulting from the presence of the absorptive inclusion depends critically on the size of the inhomogeneity. However, some important points were unresolved, such as the effectiveness of the developed perturbation approach to determine the optical characteristics of an inclusion embedded at different depths in the slab and its ability to provide the correct temporal profile of the contrast function for different longitudinal positions of the inhomogeneity.

It is the purpose of the present study to address the abovementioned points comparing model predictions with FEM simulations for an absorptive inclusion located at different depths in the scattering medium. The plan of the paper is the following. In Sec. II we will review and summarize the basic results of the first-order perturbation model to determine the change in the time-resolved transmittance resulting from the presence of a Gaussian absorptive inclusion in the coaxial detection scheme. The model is derived for a refractive index mismatch between the scattering slab and the surrounding medium through the use of the extrapolated boundary conditions. In Sec. III we will present the perturbation model based results of the time-resolved contrast and we will investigate its changes with the axial location of the inclusion. A case of practical interest, which is representative of a slightly compressed breast, will be considered to discuss numerical results [12,25]. FEM calculations will be used to validate the perturbation approach through numerical simulations of the absorptive inclusion at different depths. In Sec. IV we will show a detailed quantitative investigation of the accuracy of the perturbation model based results as a function of the axial location of the Gaussian absorptive inclusion. The relative error of the absorption perturbation parameter recovered by a fitting procedure will be calculated and discussed for different locations and for different sizes of the inclusion.

II. THEORY

The basic geometric scheme of an infinitely homogeneous extended slab is shown in Fig. 1. The perturbation model assumes a Gaussian absorptive inclusion of cylindrical shape geometry with radius R and height h being located at axial position $z=z_{pc}$ inside the scattering slab of thickness d. The spatial dependent absorption coefficient is assumed to be varying along the radial distance ρ_p according to the Gaussian law

$$\delta\mu_a(\mathbf{r_p})=\Delta\mu_a\exp\left[-2\ln 2\left(\frac{\rho_p}{R}\right)^2\right], \tag{1}$$

where $\Delta\mu_a$ is the value of the Gaussian absorptive inclusion on the cylinder axis and corresponds to the maximum deviation of the absorption coefficient from the unperturbed value μ_a of the host medium. The size of the inhomogeneity is determined by its radius R and it is defined as the radial distance at which the value of the absorption coefficient of the inclusion decreases to $\Delta\mu_a/4$.

The perturbed time-resolved transmittance $T_{pert}(t;z_{pc})$ can be written as [26]

$$T_{pert}(t;z_{pc})=T(t)+\delta T_{\mu_a}(t;z_{pc}), \tag{2}$$

where

$$T(t)=\frac{\exp(-\mu_a vt)}{4\pi A(n)Dd_e t}\sum_{m=1}^{\infty}\exp\left(-\frac{\pi^2m^2Dvt}{d_e^2}\right)\times\sin\left(\frac{m\pi(z_s+z_e)}{d_e}\right)\sin\left(\frac{m\pi(d+z_e)}{d_e}\right) \tag{3}$$

describes the basic solution of the homogeneous slab problem for an isotropic source located at a depth $z_s=1/\mu_s'$ and emitting a pulse of unit energy at time $t=0$. In Eq. (3) $D=1/3\mu_s'$ is the diffusion coefficient, μ_s' is the reduced scat-

tering coefficient of the host medium, $A(n)$ is a factor that takes into account the refractive index mismatch n between the scattering slab and the surrounding medium, $z_e = 2A(n)D$ is the extrapolated distance, and $d_e = d + 2z_e$.

In the framework of the first-order approximation to the diffusion equation we developed in Ref. [26] an analytical expression for the change $\delta T_{\mu_a}(t;z_{pc})$ in the time-resolved transmittance when a spatially varying Gaussian distributed absorptive inclusion (1) is considered, namely,

$$\delta T_{\mu_a}(t;z_{pc}) = -\frac{\Delta\mu_a}{2A(n)\pi^2 D^2 d_e^2 t} \times \sum_{k,l=1}^{\infty} \exp\left[-\mu_a v t - \frac{\pi^2 D v t (k^2+l^2)}{2d_e^2}\right] \times \mathcal{R}_{k,l}(R,t)\,\mathcal{Z}_{k,l}(z_{pc},h), \tag{4}$$

where $\mathcal{R}_{k,l}(R,t)$ is a function of the radius R of the inclusion and it is given by

$$\mathcal{R}_{k,l}(R,t) = \frac{\pi R^2 e^{-\alpha_{k,l}\beta}}{8\alpha_{k,l}\ln 2}\{[\mathrm{Ei}(\alpha_{k,l}(\beta+1)) - \mathrm{Ei}(\alpha_{k,l}(\beta-1))] + e^{2\alpha_{k,l}\beta}[\mathrm{Ei}(-\alpha_{k,l}(\beta+1)) - \mathrm{Ei}(-\alpha_{k,l}(\beta-1))]\}, \tag{5}$$

with

$$\alpha_{k,l} = \frac{\pi^2 D v t (k^2 - l^2)}{2d_e^2}, \tag{6}$$

$$\beta = \sqrt{1 + \frac{R^2}{2Dvt\ln 2}} \tag{7}$$

and the exponential integral $\mathrm{Ei}(x)$ is given by

$$\mathrm{Ei}(x) = -\int_{-x}^{\infty} \frac{e^{-y}}{y} dy,$$

where the principal value of the integral is taken.

The function $\mathcal{Z}_{k,l}(z_{pc},h)$ is given by

$$\mathcal{Z}_{k,l}(z_{pc},h) = \frac{d_e}{2\pi(k^2-l^2)} \sin\left[\frac{l\pi(d+z_e)}{d_e}\right] \sin\left[\frac{k\pi(z_s+z_e)}{d_e}\right] \times \left|(k+l)\sin\left[\frac{\pi(k-l)(z_e+z)}{d_e}\right] - (k-l)\sin\left[\frac{\pi(k+l)(z_e+z)}{d_e}\right]\right|_{z=z_{pc}-h/2}^{z=z_{pc}+h/2}. \tag{8}$$

The notation $|\cdots|_{z=z_{pc}-h/2}^{z=z_{pc}+h/2}$ means the difference of the values of the function $\mathcal{Z}_{k,l}$ between $z=z_{pc}+h/2$ and $z=z_{pc}-h/2$. It can be shown that $\mathcal{R}_{k,l}(R,t)$ and $\mathcal{Z}_{k,l}(z_{pc},h)$ reduce for $k=l$ to the following forms:

$$\mathcal{R}_{k,k}(R,t) = \frac{\pi R^2}{4\beta\ln 2}\ln\left(\frac{\beta+1}{\beta-1}\right), \tag{9}$$

$$\mathcal{Z}_{k,k}(z_{pc},h) = \frac{h}{2} + \frac{d_e}{4\pi k}\left\{\sin\left[\frac{2\pi k\left(z_e+z_{pc}+\frac{h}{2}\right)}{d_e}\right] - \sin\left[\frac{2\pi k\left(z_e+z_{pc}-\frac{h}{2}\right)}{d_e}\right]\right\}. \tag{10}$$

The dependence of the time-resolved transmittance on the longitudinal position z_{pc} of the inclusion has been explicitly introduced in the above equations because in the following section we will extensively discuss the time-resolved contrast as a function of the depth of the inclusion.

III. TEMPORAL EVOLUTION OF THE CONTRAST

The accuracy of the perturbed transmittance $T_{pert}(t;z_{pc})$ is investigated through comparisons with numerical solutions $T_{num}(t;z_{pc})$ obtained by solving the diffusion equation for the fluence rate $\Phi_{num}(\mathbf{r},t)$ in the presence of the Gaussian absorptive inhomogeneity, namely,

$$\left[D\nabla^2 - \frac{1}{v}\frac{\partial}{\partial t} - [\mu_a + \delta\mu_a(\mathbf{r})]\right]\Phi_{num}(\mathbf{r}-\mathbf{r}_s,t) = -\frac{1}{4\pi}\delta(\mathbf{r}-\mathbf{r}_s)\,\delta(t), \tag{11}$$

where $\mathbf{r}_s = (0,0,1/\mu_s')$ is the location of the source at $t=0$.

To solve numerically the diffusion equation (11) under the extrapolated boundary conditions we have employed the FEM since it has been shown to be a robust and efficient numerical method for solving the diffusion equation in the case of complex geometries and inhomogeneous media [27–29]. The numerical results refer to a diffusing slab of thickness $d=40$ mm, with the inhomogeneity located at different depth z_{pc} along the probe beam-detector z axis.

To develop a close comparison between the first-order perturbation model predictions and the FEM simulations, we have shown in Fig. 2 the temporal dependence of the contrast functions $\delta T_{pert}(t;z_{pc})/T(t)$ and $\delta T_{num}(t;z_{pc})/T(t)$ for three values z_{pc} of the location of the inhomogeneity; namely, $z_{pc}=1/4\ d$, halfway between the front surface and the central plane of the slab, $z_{pc}=1/2\ d$, at the midplane, and $z_{pc}=3/4\ d$, halfway between the central plane and the detector position.

The contrast functions are given by

$$\frac{\delta T_{pert}(t;z_{pc})}{T(t)} = \frac{T_{pert}(t;z_{pc}) - T(t)}{T(t)}, \tag{12a}$$

$$\frac{\delta T_{num}(t;z_{pc})}{T(t)} = \frac{T_{num}(t;z_{pc}) - T(t)}{T(t)}. \tag{12b}$$

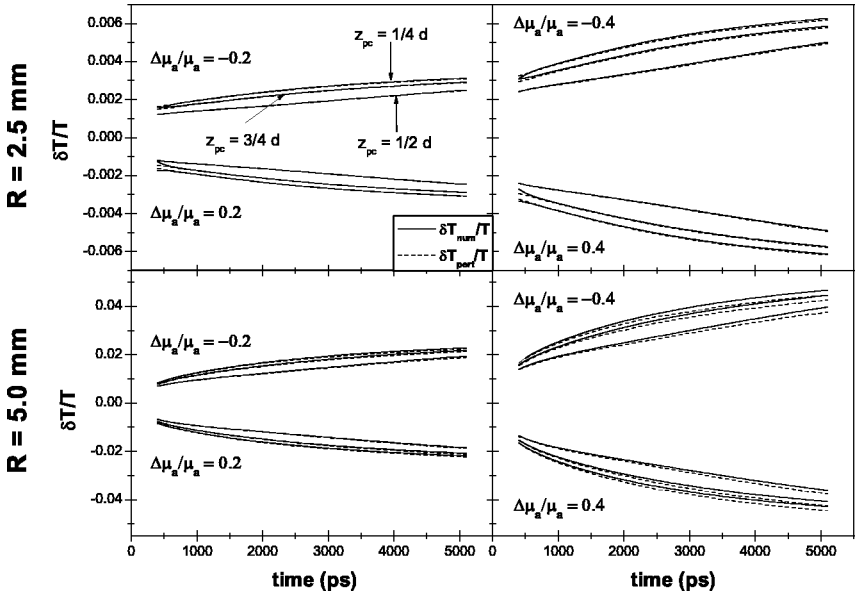

FIG. 2. Temporal behavior of the contrast functions $\delta T_{pert}(t;z_{pc})/T(t)$ and $\delta T_{num}(t;z_{pc})/T(t)$ computed at depth $z_{pc}=1/4d,1/2d,3/4d$ of the inclusion for values of the relative absorptive perturbation $\Delta\mu_a/\mu_a$ ranging from -40% to 40%. Row panels are obtained for the same value of the radius R of the inclusion, namely, $R=2.5$ mm and $R=5$ mm. Results refer to a turbid slab of thickness $d=40$ mm, relative refractive index $n=1.4$, absorption coefficient $\mu_a=0.004$ mm^{-1}, and reduced scattering coefficient $\mu_s'=1.0$ mm^{-1}.

According to Eq. (12a), $\delta T_{pert}(t;z_{pc})/T(t)$ is the relative change of the perturbed transmittance in the considered coaxial probe beam-detector configuration. Similarly, Eq. (12b) defines the relative change of the transmitted signal obtained by the FEM simulation of the Gaussian absorptive inclusion.

The temporal behavior of the contrast functions (12a) and (12b) is shown in Fig. 2 for two values of the inclusion radius, $R=2.5$ mm and $R=5$ mm. In each case, the thickness h of the cylindrical inclusion has been set equal to the diameter $2R$ [23,15,26]. The reduced scattering and the absorption coefficients of the unperturbed medium have been fixed to $\mu_s'=1.0$ mm^{-1} and $\mu_a=0.004$ mm^{-1}, respectively, and the mismatch in the refractive index has been set to the value 1.4. The considered values are of practical interest because they are representative of breast tissues [12,25]. Inspection of the curves shows that the contrast function increases as the center of the Gaussian inclusion is displaced from the central plane to the positions $z_{pc}=1/4\ d$ and $z_{pc}=3/4\ d$ that are symmetric with respect to the central plane. The perturbation model predictions $\delta T_{pert}(t;z_{pc})/T(t)$ are in excellent agreement with the FEM simulations $\delta T_{num}(t;z_{pc})/T(t)$ for $R=2.5$ mm as the relative absorptive perturbation $\Delta\mu_a/\mu_a$ ranges from -40% to 40%. Indeed, the temporal behavior of the numerically and perturbatively computed contrasts are almost indistinguishable in the considered $\Delta\mu_a/\mu_a$ range. The perturbation model generally underestimates the contrast compared to the FEM simulation, and the discrepancies remains within $\sim 5\%$ until the radius of the inhomogeneity, $R\lesssim 5$ mm. The decrease of the contrast at earlier times can be easily understood by taking into account the statistical weight factor $\exp(-\int_0^l[\mu_a+\Delta\mu_a(\mathbf{r})]dl)$ that describes the probability of survival of a photon following a trajectory of length l inside the region of the absorptive inclusion. The temporal behavior of the contrast is essentially governed by the factor $(\exp[-\int_0^l\Delta\mu_a(\mathbf{r})dl]-1)$ that decreases for photons detected at shorter times of flight, i.e., for photons that follow a trajectory close to the source-detector line. It is also clear from the

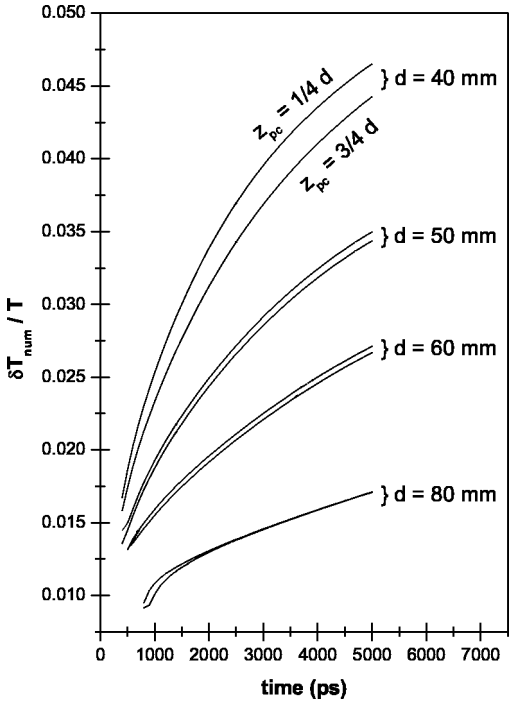

FIG. 3. The numerical contrast $\delta T_{num}(t;z_{pc})/T(t)$ at depths $z_{pc}=1/4\ d$ and $z_{pc}=3/4\ d$ for increasing values of the thickness d of the scattering slab. An absorptive inclusion with radius $R=5$ mm and negative value $\Delta\mu_a/\mu_a.=-0.4$ of the relative absorptive perturbation have been considered. The other parameters are the same as Fig. 2.

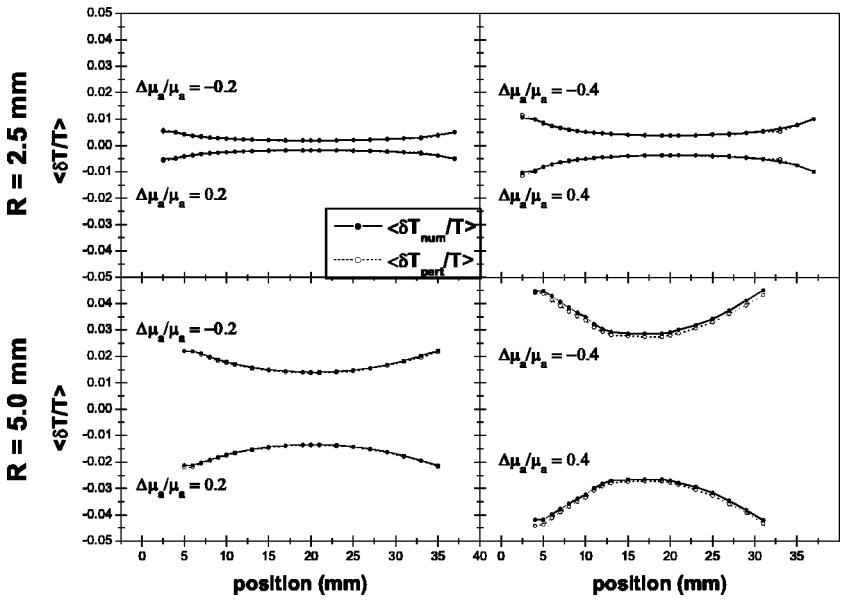

FIG. 4. Average contrast $\langle \delta T_{pert}(t;z_{pc})/T(t)\rangle$ and $\langle \delta T_{num}(t;z_{pc})/T(t)\rangle$ as function of the depth z_{pc} of the inclusion for two values of the radius R when the absorptive perturbation $\Delta\mu_a/\mu_a$ ranges from -40% to 40%. The four panels are obtained for a scattering slab with thickness $d=40$ mm, absorption coefficient $\mu_a=0.004$ mm^{-1}, reduced scattering coefficient $\mu_s'=1.0$ mm^{-1}, and refractive index mismatch $n=1.4$.

numerical results that the absolute values of the contrast computed for negative values of $\Delta\mu_a/\mu_a$ are higher than those computed for the positive values. Indeed, the quantity $(\exp[-\int_0^l \Delta\mu_a(\mathbf{r})dl]-1)$ contributes more in the former case, which causes the evident asymmetry in the temporal behavior of the contrast between positive and negative values of the relative absorptive perturbation $\Delta\mu_a/\mu_a$.

It should be noted that the values of the contrast calculated when the center of the inhomogeneity is at $z_{pc}=1/4d$ are higher than those computed with the inhomogeneity located at $z_{pc}=3/4d$. This is just a consequence of the asymmetry between source and detector locations in the considered setup. In the first case the source-inclusion distance is shorter by one scattering length $1/\mu_s'$ than the distance occurring between the inclusion and the detector in the second case. To deepen this point, let us consider the FEM simulations shown in Fig. 3. The contrast $\delta T_{num}(t;z_{pc})/T(t)$ has been computed for increasing values of the thickness d of the scattering slab with the same scattering and absorption coefficients as given for Fig. 2. A radius $R=5$ mm of the inclusion and a negative value $\Delta\mu_a/\mu_a=-0.4$ of the relative absorptive perturbation have been assumed. As we increase the thickness of the slab from $d=40$ mm to $d=80$ mm, the difference between the contrasts at $z_{pc}=1/4d$ and $z_{pc}=3/4d$ gradually reduces until the two temporal profile curves become almost indistinguishable, as can be seen by looking at the profiles computed for the thickness $d=80$ mm. Indeed, the asymmetry due to the location of the source at $z_s=1/\mu_s'$ becomes negligible with increasing the slab thickness, which makes the two contrast profiles similar as the system was truly symmetric.

IV. SPACE-DOMAIN OPTICAL CHARACTERIZATION OF THE GAUSSIAN ABSORPTIVE INCLUSION AND ACCURACY OF THE MODEL

To develop a closer analysis of the contrast dependence on the depth z_{pc} of the Gaussian absorptive inclusion we have considered the temporal averages $\langle \delta T_{pert}(t;z_{pc})/T(t)\rangle$ and $\langle \delta T_{num}(t;z_{pc})/T(t)\rangle$ of the contrast functions in the time interval of Fig. 2. Figure 4 shows the average contrast as a function of the axial location of the inhomogeneity for the same optical and geometrical parameters of Fig. 2. The perturbation model based results are in remarkable agreement with the FEM simulations. The minimum (absolute) value of the average contrast is achieved when the center of the inclusion is placed at the midplane of the scattering slab, both for positive and negative values of the relative absorptive perturbation $\Delta\mu_a/\mu_a$. For given values of the size R and of the relative absorption perturbation parameter, the average contrast tends to increase as the center of the inclusion moves closer to either one of the surfaces of the slab. For example, if we consider a radius $R=5$ mm of the inclusion and take $|\Delta\mu_a/\mu_a|=40\%$ the absolute value of the average contrast increases from 3% up to 4.5% in the considered axial range. By comparing the numerical results reported in Fig. 4 it can be clearly seen that the contrast tends to increase with increasing the radius R of the inhomogeneity and, similarly, with increasing the degree of the relative absorption perturbation $|\Delta\mu_a/\mu_a|$. In fact, higher values of R and $|\Delta\mu_a/\mu_a|$ affect photon migration more significantly, which enhances the difference between the perturbed transmitted signal and the unperturbed one. Since the accuracy of the perturbation model is expected to decrease in this condition, it is important to investigate the fitting procedure ability of

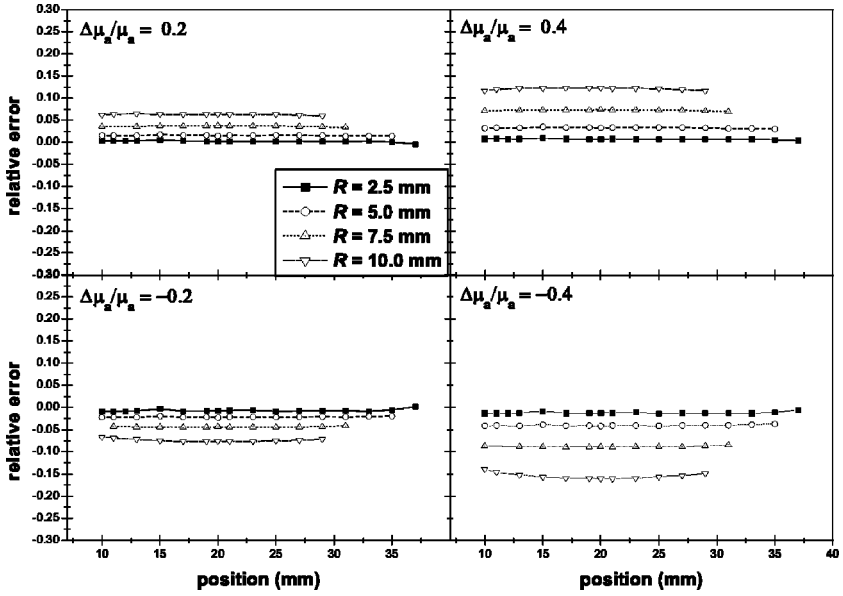

FIG. 5. Numerical calculation of the relative error $\epsilon_{\Delta\mu_a}$ as a function of the depth of the Gaussian absorptive inclusion. The four panels are obtained for a scattering slab with thickness $d=40$ mm, absorption coefficient $\mu_a=0.004$ mm^{-1}, reduced scattering coefficient $\mu_s'=1.0$ mm^{-1}, and refractive index mismatch $n=1.4$.

recovering the optical properties of the inclusion. For this purpose, the analytical model of the perturbed time-resolved transmittance, as expressed by Eqs. (2) and (4), has been implemented in a least squares fitting procedure. This permitted $T_{pert}(t;z_{pc})$ to be fitted to a FEM simulation of the time-resolved transmittance for a slab containing the Gaussian absorptive inclusion located at different depths. In the fitting procedure [30,31], only the absorptive perturbation parameter $\Delta\mu_a$ has been allowed to vary. The fitted values $\Delta\mu_{a,fit}$ have been determined for different choices of the size R and of the axial location of the inclusion.

The accuracy of the perturbation model has been investigated by calculating the relative error $\epsilon_{\Delta\mu_a}$ defined as

$$\epsilon_{\Delta\mu_a}=\frac{\Delta\mu_a-\Delta\mu_{a,fit}}{\Delta\mu_a}. \tag{13}$$

Equation (13) expresses the deviation of the fitted value $\Delta\mu_{a,fit}$ of the Gaussian absorptive inclusion from the expected one $\Delta\mu_a$ through the capability of the fitting procedure of minimizing the discrepancies between $T_{pert}(t;z_{pc})$ and $T_{num}(t;z_{pc})$. The relative error $\epsilon_{\Delta\mu_a}$ as a function of the axial location z_{pc} of the inhomogeneity is shown in Fig. 5. The numerical results have been obtained for increasing size of the inhomogeneity, ranging from $R=2.5$ mm to $R=10$ mm, and for $|\Delta\mu_a/\mu_a|=0.2$ and $|\Delta\mu_a/\mu_a|=0.4$. The absorption coefficient and the reduced scattering coefficient of the host medium are $\mu_a=0.004$ mm^{-1} and $\mu_s'=1.0$ mm^{-1}. To point out the comparison among different values of the relative error the same y scale has been adopted for each choice of R and $|\Delta\mu_a/\mu_a|$. As expected, the general behavior emerging from the results is that the relative error $\epsilon_{\Delta\mu_a}$ increases with increasing R and $|\Delta\mu_a/\mu_a|$. The worst case corresponds to the size $R=10$ mm with $|\epsilon_{\Delta\mu_a}|\simeq 18\%$ for $\Delta\mu_a/\mu_a=-0.4$. On the contrary, minimum values of the relative error are $|\epsilon_{\Delta\mu_a}|\simeq 0.6\%$ and are attained for $R=2.5$ mm and $\Delta\mu_a/\mu_a=0.2$.

It is noteworthy that the relative error does not appreciably change as we consider different axial positions of the center of the inhomogeneity although the contrast changes significantly in the considered spatial range as can be seen from the results shown in Fig. 4.

V. CONCLUSIONS

To summarize, we have performed a detailed investigation of the contrast function obtained from a first-order perturbation approach to the diffusion equation in the case of an absorptive inclusion characterized by spatially dependent Gaussian distribution of its absorption coefficient and located at different depths inside the scattering medium. We considered a slab geometry, a coaxial measurement arrangement, and a refractive index mismatch between the scattering slab and the surrounding medium. The optical parameters of the host medium were chosen so as to be representative of a slightly compressed breast. This model is expected to be more effective in realistic cases of imaging reconstruction of inhomogeneities whose optical properties change gradually from the region of the inclusion to the surrounding medium. Therefore, the considered model has a particular significance in those applications that require the detection of absorptive inclusions such as the case of many kinds of tumors in the near infrared region [32].

We have shown the time-resolved contrast increases as the inclusion moves closer to either one of the surface of the slab. The minimum value attaints with the inclusion located at the midplane. The difference among contrast values computed for inclusions located symmetrically with respect to

the midplane of the slab is due to the asymmetry between the location of the source and the detector. This difference reduces with increasing the thickness of the slab.

Perturbation model results have been analyzed through comparisons with numerical FEM solutions of the time-dependent diffusion equation. A least squares fitting procedure has been developed to recover the absorption perturbation parameter for different axial positions of the Gaussian absorptive inclusion. The numerical results have shown that the accuracy of the perturbation model is better than 20% for $|\Delta\mu_a/\mu_a|<40\%$ when the size of the inclusion is less than 10 mm and the axial location of the inhomogeneity ranges from 10 mm to 30 mm. Moreover, the relative error does not appreciably change as different axial locations of the inhomogeneity are considered. It turns out that it increases fairly regularly with increasing the size of the inclusion and the degree of the relative absorption perturbation parameter. This behavior at first-order perturbation approach might be accounted for a simple heuristic formula estimating the change of the relative error with the size and location of the inclusion and with the degree of the relative perturbation. Such a heuristic formula would be a useful figure of merit when designing optical imaging systems, and it demands further investigation in order to explore the influence of the optical properties of the host medium. It is worth pointing out that the developed perturbation model [26] and the numerical results presented so far suggest using this approach as a basic tool for inverse algorithm in order to reconstruct optical mammographic images from two-dimensional projection techniques. Furthermore, a generalization of the developed perturbation scheme to include the case of an arbitrary location of the source and of the detector with respect to that of the inhomogeneity might be conveniently used as inverse linear perturbation-based algorithm in optical tomography.

[1] *Medical Optical Tomography: Functional Imaging and Monitoring*, edited by G. Muller, R. Alfano, S. Arridge, J. Beuthan, E. Gratton, M. Kaschke, B. Masters, S. Svanberg, and P. van der Zeet, SPIE Proceedings Vol. IS 11 (SPIE, Bellingham, WA, 1993).

[2] B.W. Pogue, K. Paulsen, C. Abele, and H. Kaufman, J. Biomed. Opt. **5**, 185 (2000).

[3] J.C. Hebden, H.V.H. Dehghani, H.M.C. Hillman, M. Schweiger, S.R. Arridge, and D.T. Delpy, Appl. Opt. **40**, 3278 (2001).

[4] M. O'Leary, D. Boas, B. Chance, and A. Yodh, Opt. Lett. **20**, 426 (1995).

[5] J. Hebden, F. Schimdt, M. Fry, M. Schweiger, E. Hillman, D. Delpy, and S. Arridge, Opt. Lett. **24**, 534 (1999).

[6] H. Jiang, K. Paulsen, and U. Osterberg, Phys. Med. Biol. **41**, 1483 (1996).

[7] U. Hampel, E. Schleicher, and R. Freyer, Appl. Opt. **41**, 3816 (2002).

[8] Y. Xu, X. Gu, T. Khan, and H. Jiang, Appl. Opt. **41**, 5427 (2002).

[9] J. Ye, K. Webb, R. Millane, and T. Downar, J. Opt. Soc. Am. A **16**, 1814 (1999).

[10] W. Cai, S.K. Gayen, M. Xu, M. Zevallos, M. Alrubaiee, M. Lax, and R.R. Alfano, Appl. Opt. **38**, 4237 (1999).

[11] F. Gao, Y. Tanikawa, H. Zhao, and Y. Yamada, Appl. Opt. **41**, 7346 (2002).

[12] D. Grosenick, H. Wabnitz, H.H. Rinneberg, T. Moesta, and P.M. Schlag, Appl. Opt. **38**, 2927 (1999).

[13] J.C. Hebden and S.R. Arridge, Appl. Opt. **35**, 6788 (1996).

[14] K. Gayen and R.R. Alfano, Opt. Photonics News **7**, 17 (1996).

[15] L. Spinelli, A. Torricelli, A. Pifferi, P. Taroni, and R. Cubeddu, Appl. Opt. **42**, 3145 (2003).

[16] M.S. Patterson, B. Chance, and B.C. Wilson, Appl. Opt. **28**, 2331 (1989).

[17] S.R. Arridge, M. Cope, and D.T. Delpy, Phys. Med. Biol. **37**, 1531 (1992).

[18] D. Contini, F. Martelli, and G. Zaccanti, Appl. Opt. **36**, 4857 (1997).

[19] J.L. Karagiannes, Z. Zhang, B. Grossweiner, and L.I. Grosswiner, Appl. Opt. **28**, 2311 (1989).

[20] M. Keijzer, W.M. Star, and P. Storchi, Appl. Opt. **27**, 1820 (1988).

[21] A.G. Gandjbakhche, R.F. Bonner, R. Nossal, and G.H. Weiss, Appl. Opt. **35**, 1767 (1996).

[22] S.R. Arridge, Appl. Opt. **34**, 7395 (1995).

[23] M. Morin, S. Verrealut, A. Mailloux, J. Fréchette, S. Chatigny, Y. Painchaud, and P. Beaudry, Appl. Opt. **39**, 2840 (2000).

[24] G. Zaccanti, F. Martelli, and S.D. Bianco, Appl. Opt. **41**, 7317 (2002).

[25] S. Carraresi, T.S.M. Shatir, F. Martelli, and G. Zaccanti, Appl. Opt. **40**, 4622 (2001).

[26] S. De Nicola, R. Esposito, and M. Lepore, Phys. Rev. E **68**, 021901 (2003).

[27] S.R. Arridge, M. Schwieger, M. Hirakoa, and D.T. Delpy, Med. Phys. **20**, 299 (1993).

[28] S.R. Arridge and M. Schweiger, Appl. Opt. **34**, 8026 (1995).

[29] M. Shweiger, S.R. Arridge, M. Hiraoka, and D.T. Delpy, Med. Phys. **22**, 1779 (1995).

[30] C. P. Library, CERN Computer Center Report No. CH-1211, 1993 (unpublished).

[31] F. James and M. Rods, CERN Computer Center Report No. CH-1211, 1983 (unpublished).

[32] J.B. Fishkin, O. Coquoz, E.R. Anderson, M. Brenner, and B.J. Tromberg, Appl. Opt. **36**, 10 (1997).